

New Liquid Crystalline Conjugated Derivatives of 3,3'-Bipyridine as Components for Optoelectronic Materials

André-Jean Attias,^{*,†} Chantal Cavalli,[†] Bertrand Bloch,[†] Nathalie Guillou,[‡] and Claudine Noël[§]

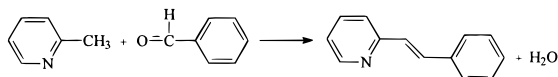
Département Matériaux et Systèmes Composites, ONERA, 29, Avenue de la Division Leclerc, B. P. 72, F-92322-Châtillon Cedex, France; Institut Lavoisier, UMR CNRS 173, Université de Versailles Saint-Quentin-en-Yvelines, 45, Avenue des Etats-Unis, F-78035-Versailles Cedex, France; and Laboratoire de Physicochimie Structurale et Macromoléculaire, URA 278, ESPCI, 10, Rue Vauquelin, F-75231-Paris Cedex 05, France

Received December 14, 1998. Revised Manuscript Received March 23, 1999

We present a series of new 6,6'-distyryl-3,3'-bipyridine derivatives synthesized via a Knoevenagel condensation reaction and disubstituted with electron donor and acceptor groups. These molecules were characterized by spectroscopic methods (NMR, Raman, UV-vis, photoluminescence). These compounds were all found to exhibit thermotropic liquid crystalline (LC) phases, the structures of which were analyzed by DSC and temperature-dependent X-ray diffraction. The high degree of conjugation and the mesogenic character of these molecules could lead to nonlinear optical (NLO) applications for the "push-pull" compounds. Absorption in the UV range and blue fluorescence are other characteristics of some members of this group. The latter property opens up applications as light-emitting diodes (LEDs).

Introduction

The Knoevenagel reaction, when applied to activated methyl derivatives of pyridine, or of other nitrogen heterocycles, directly leads, by condensation with aromatic aldehydes, to arylene-vinylene-heteroarylene bondings which may constitute the basic structural elements of entirely π -conjugated molecules.



Several other more commonly used reactional paths, like the Wittig or Heck reactions, yield similar structures, but the Knoevenagel reaction, insofar as it is a mere thermal condensation process, has the advantage of being a very simple and easy method to apply: water is the only byproduct, and there are no unstable reactive intermediates or special chemical reagents yielding reaction products that have to be eliminated.

The advantages of the pyridine moiety itself have been demonstrated on several occasions as a specially interesting structural element in optoelectronic materials, giving them peculiar properties.^{1–4} More specifically,

ly, the electron deficiency and consequently the electron affinity of the aromatic pyridine ring result in a higher resistance to oxidation and better electron transport properties, when most conjugated molecules are prone to oxidative degradation and exhibit better hole transport properties. Recent results demonstrate that pyridine-based conjugated polymers make possible the use of environmentally stable metal electrodes for the production of light-emitting diodes (LEDs).^{5–7}

The present paper is a description of a new family of conjugated molecules based on the 3,3'-bipyridine moiety, all obtained by the Knoevenagel process. Besides their optoelectronic capabilities resulting from their high conjugation level, they present a very distinctive feature, which is their ability to give rise to liquid crystalline phases.

A large part of this paper concerns the latter behavior, which was previously demonstrated as specially advantageous for second-order nonlinear optical (NLO) applications. Recently, it has been shown, both theoretically^{8,11} and experimentally,^{12–17} that particularly large

* Corresponding author. Tel: (+33) 1 46 73 45 72. Fax: (+33) 1 46 73 41 42. E-mail: attias@onera.fr.

[†] ONERA.

[‡] Université de Versailles Saint-Quentin-en-Yvelines.

[§] ESPCI.

(1) Marsella, M. J.; Fu, D. K.; Swager, T. M. *Adv. Mater.* **1995**, *7*, 145.

(2) Epstein, A. J.; Blatchford, J. W.; Wang, Y. Z.; Jessen, S. W.; Gebler, D. D.; Lin, L. B.; Gustafson, T. L.; Wang, H. L.; Park, Y. W.; Swager, T. M.; MacDiarmid, A. G. *Synth. Met.* **1996**, *78*, 253.

(3) Blatchford, J. W.; Jessen, S. W.; Lin, L. B.; Lih, J. J.; Gustafson, T. L.; Epstein, A. J.; Fu, D. K.; Marsella, M. J.; Swager, T. M.; MacDiarmid, A. G.; Yamaguchi, S.; Hamaguchi, H. *Phys. Rev. Lett.* **1996**, *76*, 1513.

(4) Bredas, J. L. Private communication.

(5) Gebler, D. D.; Wang, Y. Z.; Blatchford, J. W.; Jessen, S. W.; Lin, L. B.; Gustafson, T. L.; Wang, H. L.; Swager, T. M.; MacDiarmid, A. G.; Epstein, A. J. *J. Appl. Phys.* **1995**, *78*, 4264.

(6) Gebler, D. D.; Wang, Y. Z.; Jessen, S. W.; Blatchford, J. W.; MacDiarmid, A. G.; Swager, T. M.; Fu, D. K.; Epstein, A. J. *Synth. Met.* **1997**, *85*, 1205.

(7) Wang, Y. Z.; Gebler, D. D.; Fu, D. K.; Swager, T. M.; MacDiarmid, A. G.; Epstein, A. J. *Synth. Met.* **1997**, *85*, 1179.

(8) Meredith, G. R.; Van Dusen, J. G.; Williams, D. J. *Macromolecules* **1982**, *15*, 1385.

second-order NLO effects can be obtained by using side-chain liquid crystalline polymers (SCLCPs), in which the side groups are NLO chromophores themselves exhibiting mesogenic properties. The liquid crystalline system exhibits spontaneous axial ordering, which enhances and stabilizes the macroscopic polarization after electric field poling. It is of interest to note that the factors which enhance the hyperpolarizability β of the molecules (high aspect ratio, planarity, aromatic π -electron systems which are conjugated along the length of the molecule, charged end groups) are essentially the same as those factors which are favorable to liquid crystallinity in low molar mass compounds.^{18–21}

Initially we were encouraged to begin this study by taking advantage of results once obtained in our group²² on poly(styrylpyridine) resins (PSP). These highly thermally stable resins, used as composite matrixes, were obtained by polycondensation of methyl derivatives of pyridine, usually 2,4,6-trimethylpyridine, with terephthalaldehyde. In this case, the Knoevenagel-type condensation is made possible by the activation of the methyl groups which results from their ortho or para position with respect to the nitrogen atom. It is important to note that, in PSP resins, the formation of an arylene vinylene structure does not give rise to any conjugation between two vinylene substituents of the same pyridine ring on account of their mutual meta position.

To elaborate, by an analogous chemical process, polymers where conjugation extends over the full length of the molecule, it is necessary to start from dimethyl aromatic nitrogen bases where the position of the methyl substituents (i) is ortho or para with respect to nitrogen (to bring about reactivity) and (ii) is compliant with a para-disubstitution of the heterocyclic core in the skeleton of the resulting molecule (to establish conjugation).

An example of a molecule meeting these requirements is 2,5-dimethylpyrazine, whose condensation products with aromatic aldehydes have been reported earlier.²³ It should be noted, however, that in such styrylpyra-

zines, when exposed to light, the vinylene groups were found to cyclodimerize, resulting in linear polymers with recurring cyclobutane units in the main chain, instead of conjugated polymers.²⁴

This paper describes an alternative approach to the synthesis of conjugated poly(heteroarylene vinylene)s, whose overall strategy is based on the use of 6,6'-dimethyl-3,3'-bipyridine (**1**) as starting compound. When reacting with benzaldehyde via the Knoevenagel condensation, **1** results in a product with a conjugation length including four aryl rings and two double bonds. This product was found (i) to show absorption in the UV spectral range and an intense photoluminescence in the blue region and (ii) to possess thermotropic liquid crystalline phases. The condensation of **1** with five-member heterocyclic rings (like thiophene) or benzene rings substituted with electron acceptor and/or donor groups was subsequently exploited to fine-tune the properties of the resulting π -conjugated systems.

In this paper, we report our preliminary results on the synthesis and characterization of five new compounds (**2–6**) (Scheme 1). They are characterized by means of Raman spectroscopy, ¹H and ¹³C NMR, differential scanning calorimetry (DSC), optical microscopy, X-ray diffraction, and UV/visible and fluorescence spectroscopy. Changes in their thermal transitions, liquid crystalline behavior, and linear optical properties are analyzed and discussed in terms of substituent effects.

Experimental Section

Reagents. 2-Methyl-5-bromopyridine has been prepared by a standard method.²⁵ Benzoic anhydride, benzaldehyde, 4-cyanobenzaldehyde, 4-hexyloxybenzaldehyde, and 2-thiophenecarboxaldehyde (all from Aldrich) were used without further purification.

Syntheses. 6,6'-Dimethyl-3,3'-bipyridine (**1**). Nickel(II) chloride hexahydrate 14.16 g, (60 mmol), 62.4 g of triphenylphosphine (240 mmol), and 300 mL of *N,N*-dimethylformamide were introduced into a three-necked flask fitted with a condenser, a dropping funnel, and an argon inlet. The resulting deep blue solution was then stirred for 1 h at 50 °C, and 3.84 g of zinc powder (60 mmol) was added. After 1 h, the color of the reaction mixture changed to red brown, 10.32 g of 2-methyl-5-bromopyridine (60 mmol) was then added and the reaction progress was monitored by steric exclusion chromatography (SEC). After 8 h, 2-methyl-5-bromopyridine was consumed. The mixture was cooled to room temperature and then poured into 600 mL of a dilute ammonia solution and extracted four times with dichloromethane (4 × 120 mL). The resulting organic phase was extracted with a 2 M HCl solution (3 × 150 mL). The aqueous phase was made alkaline with a 4 M NaOH solution, and the reaction product was extracted with dichloromethane (3 × 120 mL). The organic phase was washed with water. After evaporation, 5.2 g of a crude product was purified by vacuum sublimation; 4.6 g (25.2 mmol) of pure 6,6'-dimethyl-3,3'-bipyridine (**1**) was obtained as a white pinkish powder (yield: 84%). Mp 97.4 °C. ¹H NMR (CDCl₃) δ [ppm]: 2.5 (s, 6H), 7.19 (d, 2H, ³J_{H,H} = 8.06 Hz), 7.70 (dd, 2H, ³J_{H,H} = 8.06 Hz, ⁴J_{H,H} = 2.44 Hz), and 8.65 (d, 2H, ⁴J_{H,H} = 2.44 Hz). ¹³C NMR (CDCl₃) δ [ppm]: 24.0 (CH₃), 123.2, 130.5, 134.4, 147.1, and 157.7. Anal. Calcd for C₁₂H₁₂N₂: C, 78.26; H, 6.53; N, 15.21. Found: C, 78.26; H, 6.52; N, 15.22.

(9) Singer, K. D.; Kuzyk, M. G.; Sohn, J. E. *J. Opt. Soc. Am. B: Opt. Phys.* **1987**, *4*, 968.

(10) Van der Vorst, C. P. J. M.; Picken, S. J. *Proc. SPIE* **1987**, *866*, 99.

(11) Van der Vorst, C. P. J. M.; Picken, S. J. *J. Opt. Soc. Am.* **1990**, *B7*, 320.

(12) Gonin, D.; Noël, C.; Le Borgne, A.; Gadret, G.; Kajzar, F. *Makromol. Chem., Rapid Commun.* **1992**, *13*, 537.

(13) Guichard, B.; Noël, C.; Reyx, D.; Kajzar, F. *Macromol. Chem. Phys.* **1996**, *197*, 2185.

(14) Guichard, B.; Poirier, V.; Noël, C.; Reyx, D.; Le Borgne, A.; Leblanc, M.; Large, M.; Kajzar, F. *Macromol. Chem. Phys.* **1996**, *197*, 3631.

(15) Gonin, D.; Guichard, B.; Noël, C.; Kajzar, F. In *Polymers and Other Advanced Materials: Emerging Technologies and Business Opportunities*; Prasad, P. N., et al., Eds.; Plenum Press: New York, 1995; pp 465–483.

(16) Gonin, D.; Guichard, B.; Large, M.; Dantas De Morais, T.; Noël, C.; Kajzar, F. *J. Nonlin. Opt. Phys. Mater.* **1996**, *5*, 735.

(17) Dubois, J. C.; Le Barny, P.; Mauzac, M.; Noël, C. *Acta Polym.* **1997**, *48*, 47.

(18) Barzoukas, M.; Blanchard-Desce, M.; Josse, D.; Lehn, J.-M.; Zyss, J. *J. Chem. Phys.* **1989**, *133*, 323.

(19) Cheng, L. T.; Tam, W.; Stevenson, S. H.; Meredith, G. R.; Rikken, G.; Marder, S. R. *J. Phys. Chem.* **1991**, *95*, 10631.

(20) Cheng, L. T.; Tam, W.; Marder, S. R.; Stiegman, A. E.; Rikken, G.; Spangler, C. W. *J. Phys. Chem.* **1991**, *95*, 10643.

(21) Varanasi, P. R.; Jen, A. K.-Y.; Chandrasekhar, J.; Namboothiri, I. N. N.; Rathna, A. *J. Am. Chem. Soc.* **1996**, *118*, 12443.

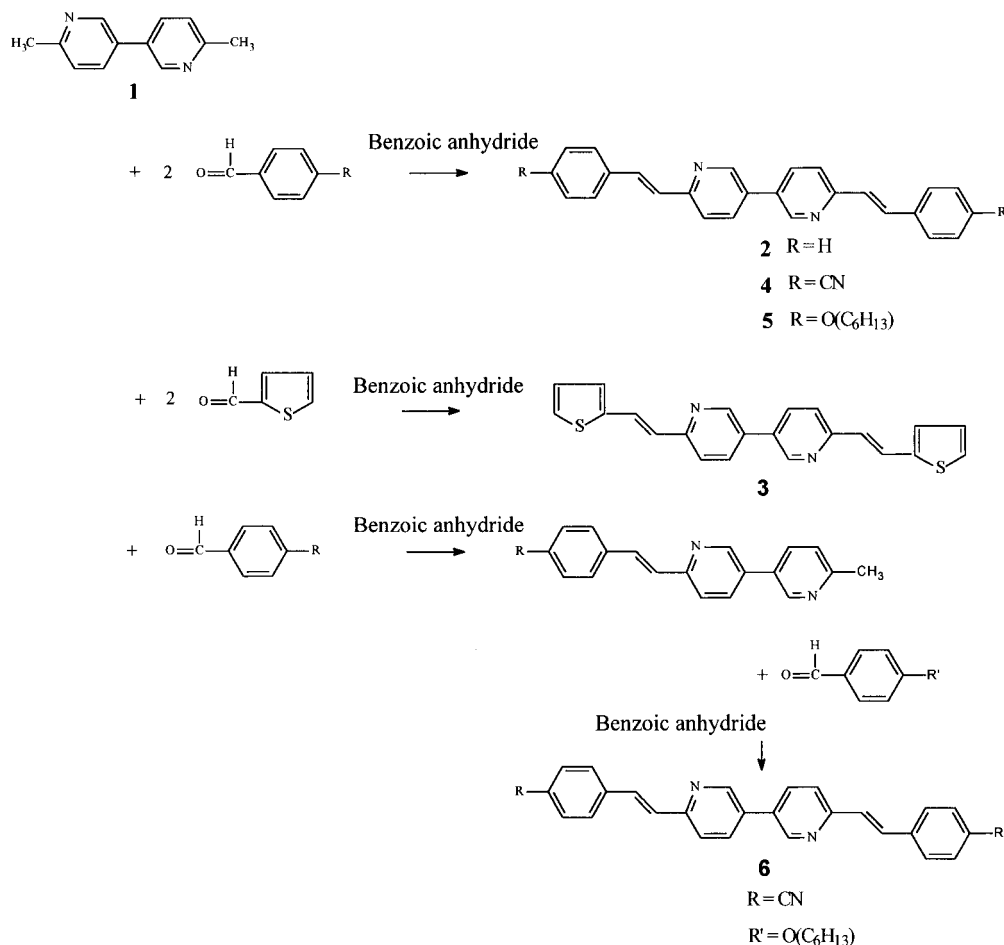
(22) Bloch, B.; Maquart, J. G. In *International Encyclopedia of Composites*; Lee, S. M., Ed.; VCH: New York, 1991; Vol. 4, 351.

(23) Nethsinghe, L. P.; Plesch, P. H.; Hodge, D. J. *Angew. Makromol. Chem.* **1987**, *148*, 161.

(24) Hasegawa, M.; Suzuki, Y.; Suzuki, F.; Nakanishi, H. *J. Polym. Sci. Part A* **1969**, *7*, 743.

(25) Pearson, D. E.; Hargrove, W. W.; Chow, J. K. T.; Suthers, B. R. *J. Org. Chem.* **1961**, *26*, 789.

Scheme 1



6,6'-Distyryl-3,3'-bipyridine (2). Compound **1** (2.7 g, 15 mmol), 6.5 g (63 mmol) of benzaldehyde, and 7.9 g (35 mmol) of benzoic anhydride were introduced into a three-necked flask fitted with a condenser, a dropping funnel, and an argon inlet. The mixture was then stirred at 200 °C and the reaction progress was monitored by SEC. After 90 min, **1** was consumed. The mixture was cooled to room temperature and washed with a 2 N NaOH solution in order to eliminate the excess of benzoic anhydride and acid formed during the reaction. The crude product was crystallized twice from toluene, and 2.03 g (5.6 mmol) of 6,6'-distyryl-3,3'-bipyridine was obtained as yellow lustrous flakes (yield: 38%). Decomposition temperature (T_d) (by TGA) = 310 °C. ^1H NMR (CDCl_3) δ [ppm]: 7.23 (d, 2H, $^3J_{\text{H,H}} = 16.0$ Hz), 7.33 (d, 2H, $^3J_{\text{H,H}} = 7.41$ Hz), 7.40 (dd, 4H, $^3J_{\text{H,H}} = 8.14$ Hz, $^4J_{\text{H,H}} = 7.41$ Hz), 7.50 (d, 2H, $^3J_{\text{H,H}} = 8.2$ Hz), 7.61 (d, 4H, $^3J_{\text{H,H}} = 8.14$ Hz), 7.70 (d, 2H, $^3J_{\text{H,H}} = 16.0$ Hz), 7.90 (dd, 2H, $^3J_{\text{H,H}} = 8.2$ Hz, $^4J_{\text{H,H}} = 2.45$ Hz), and 8.88 (d, 2H, $^4J_{\text{H,H}} = 2.45$ Hz). ^{13}C NMR (CDCl_3) δ [ppm]: 121.9, 126.9, 127.1, 128.3, 128.5, 131.2, 133.1, 134.2, 136.3, 147.5, and 154.9. Anal. Calcd for $\text{C}_{26}\text{H}_{20}\text{N}_2$: C, 86.64; H, 5.59; N, 7.77. Found: C, 86.79; H, 5.49; N, 7.72.

6,6'-Bis(2-thienylvinylene)-3,3'-bipyridine (3). This compound was prepared by the same procedure, but from 2-thiophenecarboxaldehyde (yield: 40%). $T_d = 300$ °C. ^1H NMR (CDCl_3) δ [ppm]: 7.02 (d, 2H, $^3J_{\text{H,H}} = 15.5$ Hz), 7.05 (dd, 2H, $^3J_{\text{H,H}} = 5.07$ Hz, $^3J_{\text{H,H}} = 3.3$ Hz), 7.21 (d, 2H, $^3J_{\text{H,H}} = 3.4$ Hz), 7.28 (d, 2H, $^3J_{\text{H,H}} = 5.07$ Hz), 7.41 (d, 2H, $^3J_{\text{H,H}} = 8.25$ Hz), 7.85 (d, 2H, $^3J_{\text{H,H}} = 15.53$ Hz), 7.87 (dd, 2H, $^3J_{\text{H,H}} = 8.26$ Hz, $^4J_{\text{H,H}} = 2.43$ Hz), and 8.85 (d, 2H, $^4J_{\text{H,H}} = 2.43$ Hz). ^{13}C NMR (CDCl_3) δ [ppm]: 122.1, 125.7, 126.3, 126.5, 127.8, 128.0, 131.3, 134.3, 142.1, 147.8, and 154.8. Anal. Calcd for $\text{C}_{22}\text{H}_{16}\text{N}_2\text{S}_2$: C, 70.94; H, 4.33; N, 7.52. Found: C, 71.02; H, 4.34; N, 7.43.

6,6'-Bis(4-cyanostyryl)-3,3'-bipyridine (4). This compound was prepared by the same procedure, but from 4-cyanobenzaldehyde (yield: 60%). $T_d = 380$ °C. ^1H NMR (CDCl_3) δ [ppm]:

7.31 (d, 2H, $^3J_{\text{H,H}} = 16.19$ Hz), 7.52 (d, 2H, $^3J_{\text{H,H}} = 7.88$ Hz), 7.68 (s, 8H), 7.73 (d, 2H, $^3J_{\text{H,H}} = 16.19$ Hz), 7.95 (dd, 2H, $^3J_{\text{H,H}} = 8.18$ Hz, $^4J_{\text{H,H}} = 2.4$ Hz), and 8.91 (d, 2H, $^4J_{\text{H,H}} = 2.4$ Hz). ^{13}C NMR (CDCl_3) δ [ppm]: 111.3, 118.6 (CN), 122.7, 127.3, 130.3, 131.1, 131.8, 132.3, 134.4, 140.7, 147.8, and 154.0. Anal. Calcd for $\text{C}_{28}\text{H}_{18}\text{N}_4$: C, 81.93; H, 4.42; N, 13.65. Found: C, 82.02; H, 4.33; N, 13.65.

6,6'-Bis(4-hexyloxystyryl)-3,3'-bipyridine (5). This compound was prepared by the same procedure, but from 4-hexyloxybenzaldehyde (yield: 35%). ^1H NMR (CDCl_3) δ [ppm]: 0.91 (t, 6H, $^3J_{\text{H,H}} = 7.1$ Hz), 1.34 (m, 8H), 1.45 (m, 4H), 1.78 (m, 4H), 3.98 (t, 4H, $^3J_{\text{H,H}} = 6.7$ Hz), 6.92 (d, 4H, $^3J_{\text{H,H}} = 8.78$ Hz), 7.08 (d, 2H, $^3J_{\text{H,H}} = 16.02$ Hz), 7.44 (d, 2H, $^3J_{\text{H,H}} = 8.38$ Hz), 7.53 (d, 4H, $^3J_{\text{H,H}} = 8.78$ Hz), 7.66 (d, 2H, $^3J_{\text{H,H}} = 16.02$ Hz), 7.86 (dd, 2H, $^3J_{\text{H,H}} = 8.31$ Hz, $^4J_{\text{H,H}} = 2.18$ Hz), and 8.84 (d, 2H, $^4J_{\text{H,H}} = 2.18$ Hz). ^{13}C NMR (CDCl_3) δ [ppm]: 13.8, 22.3, 25.5, 29.0, 31.3, 67.9, 114.8, 121.7, 124.9, 128.5, 129.1, 131.0, 132.9, 134.3, 147.6, 155.5, and 159.6. Anal. Calcd for $\text{C}_{38}\text{H}_{44}\text{N}_2\text{O}_2$: C, 81.39; H, 7.91; N, 5.0. Found: C, 81.45; H, 7.99; N, 4.86.

6-(4-Cyanostyryl)-6'-(4-hexyloxystyryl)-3,3'-bipyridine (6). This compound was prepared by the same procedure, but the synthesis was conducted in two steps, with equimolecular proportion of, successively, 4-cyanobenzaldehyde and 4-hexyloxybenzaldehyde. The intermediate monostyryl compound resulting from the condensation of **1** with 4-cyanobenzaldehyde (1/1 mol/mol) was isolated by dissolution in ethanol and purified before the condensation with 4-hexyloxybenzaldehyde (1/1 mol/mol) (yields: step 1, 35%; step 2, 28%). ^1H NMR (CDCl_3) δ [ppm]: 0.91 (t, 3H, $^3J_{\text{H,H}} = 7.1$ Hz), 1.35 (m, 4H), 1.47 (m, 2H), 1.8 (m, 2H), 3.99 (t, 2H, $^3J_{\text{H,H}} = 6.65$ Hz), 6.91 (d, 2H, $^3J_{\text{H,H}} = 8.43$ Hz), 7.08 (d, ^1H , $^3J_{\text{H,H}} = 16.1$ Hz), 7.29 (d, ^1H , $^3J_{\text{H,H}} = 16.3$ Hz), 7.45 (d, ^1H , $^3J_{\text{H,H}} = 8.4$ Hz), 7.49 (d, ^1H , $^3J_{\text{H,H}} = 8.4$ Hz), 7.53 (d, 2H, $^3J_{\text{H,H}} = 8.43$ Hz), 7.66 (d, ^1H , $^3J_{\text{H,H}} = 16.1$ Hz), 7.67 (s, 4H), 7.7 (d, ^1H , $^3J_{\text{H,H}} = 16.0$ Hz), 7.87 (dd, ^1H , $^3J_{\text{H,H}} = 8.15$ Hz, $^4J_{\text{H,H}} = 2.4$ Hz), 7.92 (dd, ^1H , $^3J_{\text{H,H}} = 8.15$

Hz, $^4J_{\text{H,H}} = 2.4$ Hz), 8.85 (d, ^1H , $^4J_{\text{H,H}} = 2.7$ Hz), and 8.89 (d, ^1H , $^4J_{\text{H,H}} = 2.4$ Hz). ^{13}C NMR (CDCl_3) δ [ppm]: 13.8, 22.3, 25.5, 29.0, 31.3, 67.9, 111.3, 114.6, 118.6 (CN), 121.6, 122.7, 124.6, 127.3, 128.3, 128.7, 130.4, 130.5, 130.8, 132.2, 132.3, 133.0, 134.2, 134.3, 140.8, 147.5, 147.7, 153.6, 155.6, and 159.5. Anal. Calcd for $\text{C}_{33}\text{H}_{31}\text{N}_3\text{O}$: C, 81.62; H, 6.43; N, 8.65. Found: C, 81.62; H, 6.48; N, 8.60.

Techniques. Nuclear Magnetic Resonance (NMR) Spectroscopy. ^1H and ^{13}C NMR spectra were recorded on a Varian Unity 300 spectrometer operating at 299.95 and 75.144 MHz, respectively. Chloroform-*d* (CDCl_3) was used as solvent and tetramethylsilane (TMS) as internal standard.

Raman Spectroscopy. Raman spectra were recorded on a Perkin-Elmer 2000-FT spectrometer, using the 1.064 μm line of a Nd :YAG laser beam.

Thermal Analysis. The transition temperatures were measured using a differential thermal analyzer (Dupont 1090) operating at 20 $^\circ\text{C}/\text{min}$ under nitrogen.

Thermogravimetric Analysis (TGA). Thermal stabilities were assessed by thermogravimetry (thermogravimetric analyzer Dupont 950) carried out under argon at 5 $^\circ\text{C}/\text{min}$. T_d corresponds to 5% weight loss.

X-ray Diffraction. Precise powder diffractograms were collected with a Siemens D5000 powder diffractometer equipped with a secondary monochromator using a Cu K α radiation ($\lambda = 1.5418$ Å).

The temperature-dependent X-ray diffractograms (TDXD) were recorded in air using a Siemens D5000 instrument, equipped with a M Braun linear position sensitive detector (PSD) ($\lambda = 1.7903$ Å, Co K α) and an Anton Paar (HTK 16) high-temperature chamber.

X-ray diffraction patterns were recorded on flat films using Cu K α radiation ($\lambda = 1.54056$ Å). A flat graphite crystal with a pinhole collimator was used as a monochromator. The samples were introduced in 1 mm Lindemann glass tubes which were put in an electrically heated oven, the temperature of which was controlled within 0.2 $^\circ\text{C}$ using a platinum resistor as a sensing element.

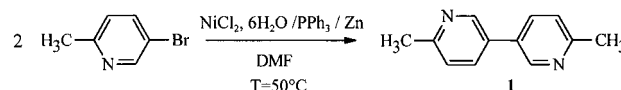
Phase Behavior. Optical textures were observed under a polarizing microscope (Olympus BHA-P) equipped with a Mettler FP52 hot-stage and FP 5 control unit, or a Leitz 350 microscope (Ernst Leitz, Wetzlar) for observations in the temperature range 300–350 $^\circ\text{C}$.

Optical Spectroscopies. The UV–visible absorbance spectra for compounds 2–6 were obtained from their solutions in a toluene/acetonitrile (50/50 v/v) mixture using a diode array spectrophotometer (J. M. Analytische Mess und Regeltechnik GmbH, Aalen, Germany). A 1 cm quartz cell was used. The concentrations were chosen so that appropriate absorbance values ($\text{OD} = 0.1$ – 0.2) were obtained at λ_{max} . The fluorescence and excitation spectra were obtained from the same solutions, using a Aminco-Bowman Series 2 luminescence spectrometer. Fluorescence quantum yields were measured in toluene/acetonitrile (50/50 v/v) solutions by comparison with the emission of quinine sulfate (in aqueous sulfuric solution) for which a value 0.55 has been taken. Quantum yields were not corrected for the change in refractive index between the toluene/acetonitrile (50/50 v/v) solutions and aqueous sulfuric solution.

Results and Discussion

Synthesis. 6,6'-Dimethyl-3,3'-bipyridine (**1**) was first synthesized according to the only published procedure for this compound, described by Peake et al.,²⁶ which is based on a nucleophilic addition of methyllithium on pyridine with subsequent regeneration of the aromatic system and homocoupling in the presence of iodine. The use of a lithium derivative required drastic experimental conditions. In addition, this method gave a low yield (15%). This prompted us to use a simpler and higher-yield synthesis of bipyridines which consisted of the homocoupling of halopyridines mediated by nickel–

Scheme 2



phosphine complexes.²⁷ We have adapted this method to the case of the synthesis of (**1**), by using 2-methyl-5-bromopyridine as starting material (Scheme 2).

All the symmetrical disubstituted compounds (**2**–**5**) were prepared according to the procedure described by Hasegawa et al.²⁴ which involved condensation of **1** with excess aromatic aldehyde at reflux temperature in the presence of benzoic anhydride. The synthesis of the donor–acceptor unsymmetrically para-disubstituted compound **6** was conducted in two stages. **1** was first reacted with 4-cyanobenzaldehyde as described before, except that equimolar amounts of reagents were used. After separation and purification, taking advantage of differences of solubility in alcohol, the resulting monostyryl compound was then reacted with 4-hexyloxybenzaldehyde, affording **6**.

Chemical Structure. The chemical structures of compounds **2**–**6** were investigated by Raman and ^1H and ^{13}C NMR spectroscopies. Raman spectra were obtained using the 1064 nm line of a Nd:YAG laser in order to avoid fluorescence.

A representative Raman spectrum is displayed in Figure 1S of the Supporting Information for a solid sample of **4**. Significant features of this Raman spectrum are the well-isolated and very characteristic band due to the stretching of the terminal C=N group at 2222 cm^{-1} and the band at 1636 cm^{-1} , which is analogous to the olefin double bond stretch at 1639 and 1632 cm^{-1} in *trans*-stilbene and *trans*-4,4'-diphenylstilbene, respectively.²⁸

Because of the low solubility of some of the compounds under interest, ^{13}C NMR spectra were obtained using the INEPT pulse sequence²⁹ with a view to enhancing the signal of the ^{13}C by polarization-transfer from the ^1H . The use of a one-bond ($^1J_{\text{CH}}$) coupling constant ($J = 165$ Hz) gives spectra revealing the protonated carbons, as shown in Figure 2Sa of the Supporting Information for compound **4**. Comparison of these spectra with the ones obtained by using a geminal ($^2J_{\text{CH}}$) or vicinal ($^3J_{\text{CH}}$) coupling constant ($J = 13$ Hz) brings out the quaternary carbons (Figure 2Sb).

The ^1H and ^{13}C NMR data (chemical structure, numbering scheme, and chemical shifts) are summarized in Tables 1 and 2, respectively. The assignments of the peaks, based on values resulting from increment predictions,³⁰ are consistent with the expected structures for compounds **2**–**6**. The presence of *trans*-vinylene units is clearly revealed in the ^1H NMR spectra. For example, in the spectrum of **5** (Figure 1), two doublets appear at 7.08 and 7.66 ppm with a three-bond coupling constant $^3J_{\text{H,H}} = 16$ Hz, indicative of a

(26) Peake, D. A.; Oyler, A. R.; Heikkilä, K. E.; Liukkonen, R. J.; Engroff, E. C.; Carlson, R. M. *Synth. Commun.* **1983**, *13*, 21.

(27) Tiecco, M.; Testaferri, L.; Tingoli, M.; Chianelli, D.; Montanucci, M. *Synthesis* **1984**, *9*, 736.

(28) Butler, R. M.; Matthew, A.; Lynn, M. A.; Gustafson, T. L. *J. Phys. Chem.* **1993**, *97*, 2609.

(29) Morris, G. A.; Freeman, R. *J. Am. Chem. Soc.* **1979**, *101*, 760.

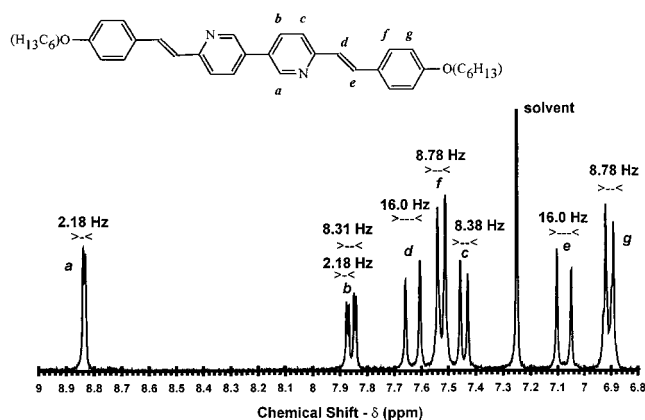
(30) Breitmaier, E.; Voelter, W. *Carbon-13 NMR Spectroscopy*; VCH: New York, 1987.

Table 1. Assignments and Chemical Shifts (ppm) of ^1H NMR Spectra Compounds 1–6

Compound	H_a	H_b	H_c	$\text{H}_d\text{--H}_e$	$\text{H}_f\text{--H}_g$	H_h
	$\text{H}_{a'}$	$\text{H}_{b'}$	$\text{H}_{c'}$	$\text{H}_{d'}\text{--H}_{e'}$	$\text{H}_{f'}\text{--H}_{g'}$	$\text{H}_{h'}$
δ (ppm)						
	1	8.65	7.7	7.19		
	2	8.88	7.9	7.5	7.70-7.23	7.61-7.40 7.33
	3	8.85	7.87	7.41	7.85-7.02	7.21-7.05 7.28
	4	8.91	7.95	7.52	7.73-7.31	7.68
	5	8.84	7.86	7.44	7.66-7.08	7.53-6.92
	6	8.89 8.85	7.92 7.87	7.49 7.45	7.70-7.29 7.66-7.08	7.67 7.53-6.91

trans carbon-carbon double bond. Spectra of all the other compounds present the same features.

As can be seen in Table 1, substitution by phenyl (2) or thienyl (3) rings results in a downfield shift of the signals of the protons of the pyridine rings, the effect being more pronounced in the case of the phenyl ring. Examination of Table 1 also reveals that symmetrical para-disubstitution of (2) by electron acceptor (4) or electron donor (5) groups leads to deshielding or shielding of the protons of the pyridinic rings, respectively. The same effect is observed for the protons of the vinylene group. These results indicate that the conjugation path goes at least from the aryl ring to the nearest pyridine ring through the *trans*-vinylene bond.

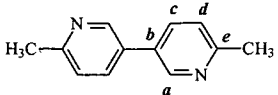
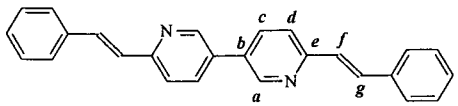
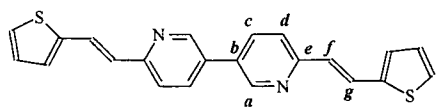
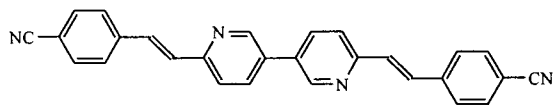
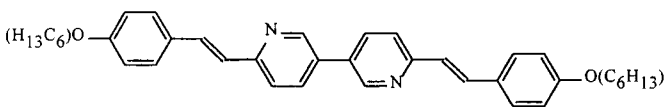
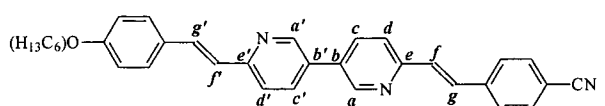
Figure 1. ^1H NMR spectrum of **5** in CDCl_3 .

The comparison of results obtained for the asymmetrically (donor/acceptor) para-disubstituted compound **6** with those for the symmetrically acceptor (4) or donor (5) disubstituted ones is more revealing. Replacing, in one phenyl end of **4**, a $-\text{CN}$ acceptor substituent by a OC_6H_{13} donor group (giving **6**) induces an upfield shift of the proton signals up to the farthest pyridylene and vinylene groups. From the data obtained for **5** and **6**, it seems that the effect is opposite and much smaller (at the limit of the experimental accuracy) when a donor group of **5** is replaced by an acceptor substituent. These results suggest that for the 6,6'-distyryl-3,3'-bipyridine derivatives, the conjugation occurs throughout the whole molecule. Similar conclusion can be drawn from the ^{13}C NMR data given in Table 2.

Mesomorphic Behavior. All compounds were examined by DSC. Representative DSC traces are given in parts a, b, and c of Figure 2 for compounds **2**, **5**, and **6**, respectively. The transition temperatures and the corresponding enthalpy changes are listed in Table 3. The lengths (L) of the molecules in the fully extended all-*trans* conformation are determined from their optimized geometry calculated at AM1 or PM3 levels.

Compound 2. Compound **2** exhibits a crystalline (K), a smectic A (S_A), a nematic (N), and an isotropic phase. The initial room-temperature X-ray diffraction pattern is consistent with a crystalline or 3D ordered smectic phase. It shows several well-defined rings corresponding to the following lattice spacings: 18.28 (vs), 9.18 (m), 6.125 (s), 4.60 (s), 4.555 (w), 4.365 (w), 3.84 (w), and

Table 2. Assignments and Chemical Shifts (ppm) of ^{13}C NMR Spectra of Compounds 1–6

Compound	C_a	C_b	C_c	C_d	C_e	C_f	C_g
	$\text{C}_{a'}$	$\text{C}_{b'}$	$\text{C}_{c'}$	$\text{C}_{d'}$	$\text{C}_{e'}$	$\text{C}_{f'}$	$\text{C}_{g'}$
(ppm)							
	147.1	130.5	134.4	123.2	157.7		
	147.5	131.2	134.2	121.9	154.9	128.3	133.1
	147.8	131.3	134.3	122.1	154.8		
	147.8	131.8	134.4	122.7	154.0	130.3	131.1
	147.6	131.0	134.3	121.7	155.5	124.9	132.9
	147.7	132.2	134.3	122.7	153.6	130.5	130.8
	147.5	130.4	134.2	121.6	155.6	124.6	133.0

3.07 Å (w). From these data alone, it is not possible to propose unit cell parameters. It should be noted, however, that the first three orders of reflection correspond to a repeat distance $d = 18.3\text{--}18.4$ Å, which is smaller than the length of the molecule in the fully extended all-trans conformation ($L = 22.3$ Å). This implies that the constituent molecules of the crystalline phase are tilted at an angle $\theta \approx 34\text{--}35^\circ$.

The X-ray patterns do not change significantly with increasing temperature up to 230 °C, a temperature close to the maximum of the first DSC endotherm (Figure 2a), which corresponds to the melting point. A further increase in temperature results in a transformation of the X-ray patterns. Clearly, the melt orients under the influence of flow with the director parallel to the Lindemann tube axis. The resulting X-ray patterns are qualitatively the same as those for oriented samples of low-molar mass smectic A phases. The anisotropy is clearly shown (Figure 3) and there are correlations of two distinct periods, parallel and perpendicular to the director, which correspond to an average molecular width (≈ 4.56 Å) and layer thickness ($d \approx 24.3\text{--}24.9$ Å), respectively. The two symmetrical wide-angle crescents are associated with the unstructured liquid-like nature of the layers. The four small-angle Bragg spots show the existence of extensive layer-like correlations and correspond to the two first orders of reflection on the layer planes. The relative position of the wide-angle crescents and the small-angle reflections indicate that the molecules tend to be orthogonal to the layer planes. The lamellar spacing (d) is slightly larger than the

extended molecular length (L); the ratio d/L is on the order of 1.1, which suggests a bilayer structure in which there is a nearly complete overlap of the molecules. However, those A type smectogens that are known to have interdigitated bilayer structures appear to have molecular structures that incorporate a terminal strong dipolar group, such as a cyano or nitro substituent. Alternatively, the small difference of ca. 2 Å between d and L might arise from the mean thermal displacement of the molecules along the director. The X-ray study of the nematic phase was not possible because of the high value of the S_A/N transition temperature (Table 3); during the time required to record the scattered intensity, degradation occurred.

Figures 4 and 5 present the mesomorphic textures of compound 2 observed under a polarizing microscope. Above its melting point, 2 gives a clear focal-conic fan texture, which exhibits characteristic features of S_A phases. Upon passing to the high-temperature mesophase, a Schlieren texture forms. From the observation of disinclinations of strength $s = \pm 1/2$, this mesophase can be unambiguously identified as a nematic phase.

Compound 3. Compound 3, in which the two phenyl rings are replaced by thienyl rings, exhibits three crystalline modifications and a nematic phase. The crystalline forms are clearly evidenced by X-ray data (Figure 6). However, the X-ray investigation did not yield conclusive information about the mesophase because specimen degradation occurred too rapidly above the melting point. To minimize in situ specimen deg-

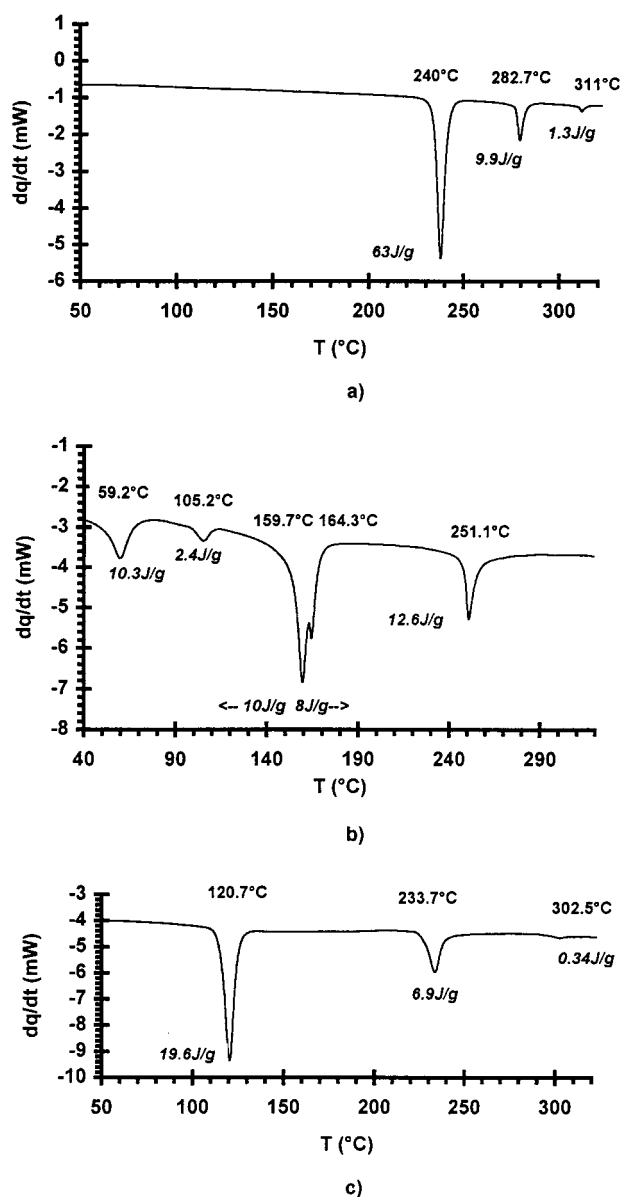


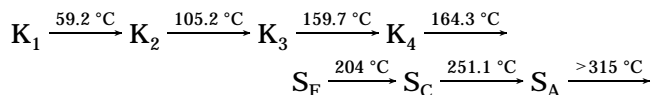
Figure 2. DSC traces: (a) **2**, (b) **5**, and (c) **6**.

radiation during the optical observations, the hot-stage was preheated to 250 °C before the sample was mounted and heated to 280 °C at 20 °C/min. At about 260–265 °C, compound **3** melts to give a nematic phase which exhibits the unmistakable Schlieren texture. Thin layers display other nematic characteristics, such as scintillation effects or a sparkling phenomenon and a marked tendency to be homeotropic, the molecules aligning with an average orientation perpendicular to the glass surfaces. At approximately 285 °C, the first drops of isotropic liquid appear, in agreement with the small endotherm observed between 285 and 295 °C in the DSC curve (Table 3).

Compound 4. Compound **4**, with terminal ring CN groups, exhibits two crystalline modifications, which are clearly evidenced by X-ray data (Figure 7), and a nematic phase, which shows readily identifiable threaded and Schlieren textures, according to whether a thick or thin film preparation is used, respectively. Two types of disinclination are observed, one with strength $s = \pm 1/2$ and one with strength $s = \pm 1$. The former dominates at lower temperatures. However, more and more dis-

inclinations of strength $s = \pm 1$ form as the temperature is increased. Simultaneously scintillation effects can be observed. At about 345–350 °C, the first drops of isotropic liquid appear. On cooling, the nematic phase separates from isotropic liquid in the form of typical droplets, which then coalesce and build up the Schlieren texture. Symmetrical para-disubstitution of **2** by CN groups raises the melting point by about 72 °C and increases the liquid crystal/isotropic transition temperature even more (>350 °C). These results show the very powerful effect of the CN group in enhancing nematic thermal stability. It is tempting to relate this to the fact that ring CN groups have strong dipoles which lie along the long molecular axis. Such dipoles have been envisaged³¹ as causing repulsions between molecules which lie parallel to one another, i.e., side by side, thus destabilizing smectic molecular arrangements.

Compound 5. DSC (Figure 2b) and X-ray data (Figure 8 and Table 4) make evident that compound **5**, while heated, exhibits a multiplicity of phase transitions. A close analysis of these data, hereunder detailed, leads to the conclusion that the following phases sequence is involved:



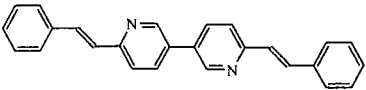
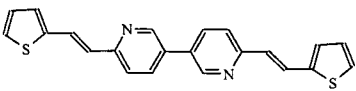
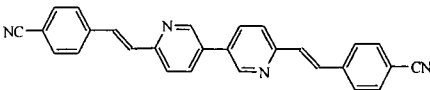
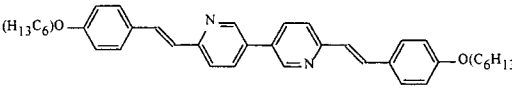
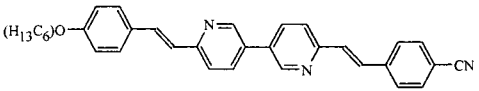
The four crystalline (or 3D ordered smectic) modifications are clearly evidenced by DSC and X-ray diffraction. It is worth noting that in the temperature range of the K_3 phase (105–159 °C) the angular positions in the X-ray patterns and the relative intensities of the wide-angle reflections corresponding to spacing 4.51 and 3.96 Å are in agreement with the data reported by Doucet et al. for low mass smectic E (S_E) phases.³² Therefore, these reflections could be tentatively indexed as the 110 and 200 reflections of a two-dimensional pseudorectangular lattice with cell parameters $a = 7.92 \pm 0.1$ Å and $b = 5.5 \pm 0.5$ Å. The a/b ratio is ≈ 1.44 , which differs noticeably from an ideal hexagonal arrangement of the molecules characterized by $a = b\sqrt{3}$. This is consistent with most results reported so far for S_E phases. Usually, powder patterns of the crystal-like S_E phase display hkl reflections very close to the $hk0$ ones. The other hkl reflections remain mostly undetected on such patterns.^{32,33} The presence of the reflection at 4.26 Å (Table 4), which could be indexed as 112 reflection, would confirm the attribution of a S_E phase (crystal-like phase) to the K_3 phase under investigation. In addition, the X-ray patterns are characterized in the small-angle region by three peaks, namely a third-order reflection, 003; a fourth-order reflection, 004; and a fifth order reflection, 005. They correspond to a Bragg spacing of $d \approx 34.13$ Å, which is close to the extended molecular length, $L = 35.10$ Å. Upon heating compound **5** for the first time, between crossed polarizers, no fluidity can be detected below 160 °C. At this temperature, the onset

(31) Gray, G. W. Influence of Composition and Structure on the Liquid Crystals Formed by Non-Amphiphilic Systems. In *Liquid Crystals*; Gray, G. W., Winsor, P. A., Eds.; Ellis Horwood Limited: Chichester, 1974; pp 103–152.

(32) Doucet, J.; Levelut, A. M.; Lambert, M.; Liebert, L.; Strzelecki, J. *J. Phys. Colloq. Fr.* **1975**, *36*, C1–13.

(33) Doucet, J.; Levelut, A. M. *J. Phys. (Paris)* **1977**, *38*, 1163.

Table 3. Phases Transitions of Compounds 2–6

Compound	Phase - Transition Temperature (°C) - [Enthalpy Change ΔH (J/g)] ^a
	2 K 240 [62.92] S _A 282.7 [9.9] N 315.1 [1.3] I
	3 K ₁ 125.3 [11.7] K ₂ 249.9 [25.4] K ₃ 263.4 [57.7] N 291.3 [1.8] I
	4 K ₁ 279 [2.7] K ₂ 311.9 [93.6] N >350 I
	5 K ₁ 59.2 [10.3] K ₂ 105.2 [2.4] K ₃ 159.7 ^b K ₄ 164.3 ^b S _F 204 ^c S _C 251.1 [12.6] S _A >315 I
	6 K 120.7 [19.5] S _{x1} ^e 185–205 ^d S _{x2} ^e 233.7 [6.9] N 302.5 [0.34] I

^a Determined by DSC. ^b The enthalpy change cannot be determined because of the overlapping of the K₃/K₄ and K₄/S_F transitions. ^c Very small endotherm. ^d Undetected by DSC, but evidenced by optical microscopy and X-ray diffraction. ^e S_{x1} and S_{x2} could be tentatively identified as a smectic B and a smectic A phase, respectively, from the results obtained by optical microscopy and X-ray diffraction (see the text).

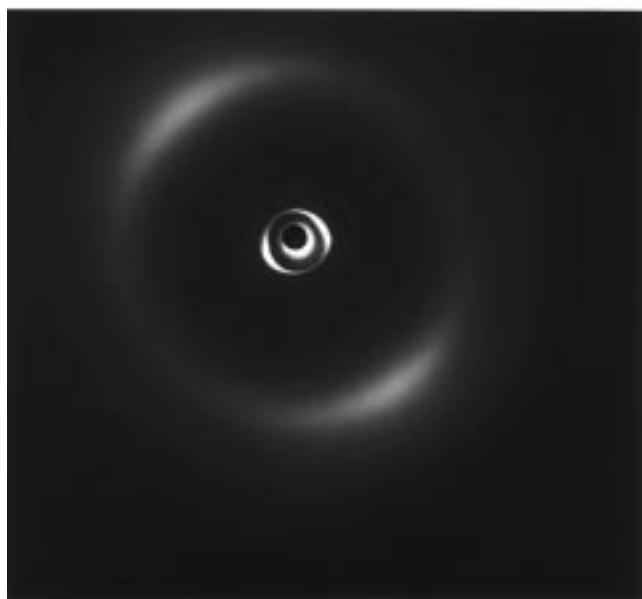


Figure 3. Diffraction pattern for an oriented sample of the S_A phase of compound **2**.

of melting occurs, but the material displays a high viscosity and produces an ill-defined texture which does not reveal any particular morphological feature useful for phase identification.

Over the temperature range 180–210 °C, the viscosity decreases and homogeneous domains form in which lines (looking like a string of pearls) that are sets of small focal conics can be observed. In the thin portions of the preparation, a Schlieren texture develops as the



Figure 4. The focal conic fan texture of the S_A phase of **2** (crossed polarizers, magnification 200×).

temperature increases from 210 to 250 °C. This Schlieren texture exhibits only singularities with $s = \pm 1$, which is consistent with a smectic C (S_C) phase.

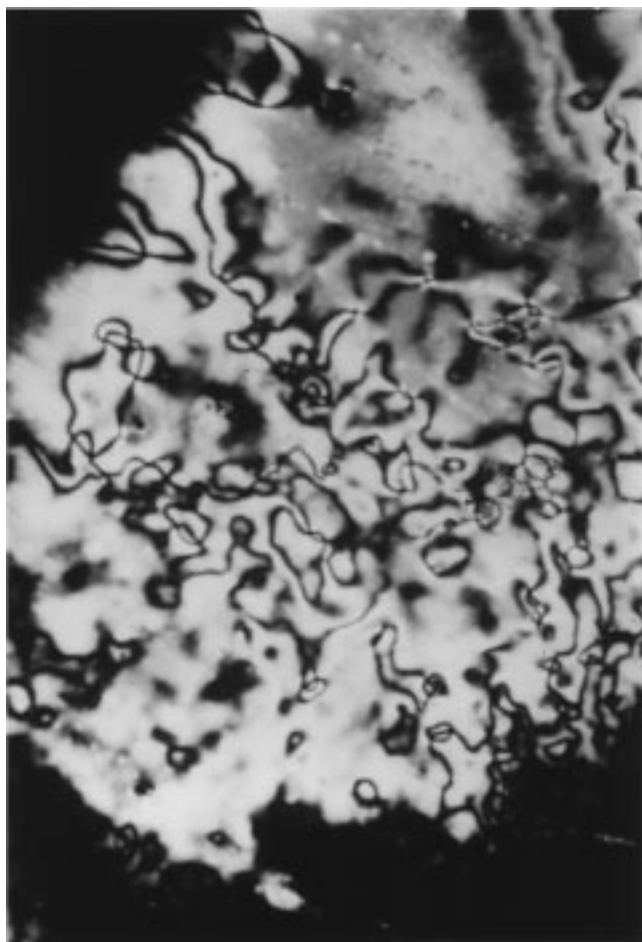


Figure 5. The Schlieren texture of the nematic phase of **2** (crossed polarizers, magnification 200 \times).

Over the temperature range 250–270 °C textural changes occur, indicating the existence of a S_A phase. When thick-film preparation is used, it exhibits a polygonal texture. Fan-shaped textures appear in thinner specimens. Variants with spherulitic domains or ellipses of different dimensions are also observed, depending on the experimental conditions. Simultaneously, homeotropic texture is obtained from the Schlieren texture. The S_A /isotropic liquid transition is undetected by optical microscopy up to ca. 315 °C, the temperature at which sublimation and degradation of compound **5** occur.

Upon cooling from the S_A phase, the S_C phase shows the broken polygonal or fan-shaped texture and the Schlieren texture. The S_C / S_F transition is clearly observed. The Schlieren areas are still retained, but the texture is now crossed with fine mosaic lines, giving a Schlieren–mosaic texture. Simultaneously, the fan texture shows breakages, although in a limited number.

Confirmation of the identification of the S_F and S_C phases was obtained by X-ray diffraction (Figure 8 and Table 4). In the S_C phase, X-ray diffraction patterns show a diffuse halo, which is related to lateral interactions between the mesogenic cores and corresponds to an average molecular spacing of ca. 4.45–4.55 Å, and a small peak ($d = 11.04$ Å), which indicates the existence of extensive layer-like correlations and can be indexed as the 003 reflection on the layer planes. The layer thickness ($d = 33.12$ Å) is smaller than the extended

molecular length ($L = 35.10$ Å), showing that the molecules are tilted with respect to the normal to the layer planes. The tilt angle θ ($\cos \theta = d/L$) is about 19°30' at 215 °C. In the S_F phase the X-ray diffractograms are similar to those of the S_C phase, except that the diffuse halo is replaced by a broad peak, indicating that now the mesogenic cores are packed in a hexagonal array. The layer thickness is $d = 32.46$ Å at 190 °C, which corresponds to a tilt angle $\theta = 22°30'$ ($d = 31.62$ Å at 180 °C, $\theta = 26^\circ$). It should be noted that the appearance of the S_F phase is accompanied by a jump in the value of the lamellar spacing. Such an effect seems to be a general feature of the S_F (or S_I)/ S_C transition in low molar mass LCs.^{34,35} The X-ray investigation did not yield conclusive information about the S_A phase because decomposition and sublimation of the specimen occurred during the time required to record the scattered intensity.

All these results confirm information about the effects of terminal substituents on liquid crystal properties which have been obtained by studying mesogenic compounds differing only in the nature of their substituents.³¹ It has been found that while certain terminal ring X substituents, e.g., X = long *n*-alkyl chains, favor smectic thermal stabilities, others, e.g., X = CN, markedly enhance nematic and diminish smectic thermal stabilities. The results in Table 3 show that these effects are also observed for compounds **4** and **5**. Compound **5** is purely smectogenic.

Compound 6. The very powerful effects of the CN group and *n*-hexyl group in promoting nematic and smectic phase formation, respectively, are highlighted by the fact that the unsymmetrically para-disubstituted compound **6** exhibits, in addition to a crystalline (or 3D ordered smectic), a nematic (N), and two smectic not immediately identifiable phases (S_{x1} and S_{x2}) (Table 3).

Upon heating compound **6** for the first time, no fluidity can be detected by optical microscopy below 110–130 °C. In this temperature range, which corresponds to the first DSC endotherm (Figure 2c), melting occurs. However, the material displays high viscosity and no typical texture can be induced. Over the temperature range 185–195 °C (i.e., S_{x1}/S_{x2} transition), although no transition appears in the DSC trace (Figure 2c), the viscosity decreases slightly and the ill-defined texture is progressively replaced by sets of small conics and spherulites. Simultaneously, the thinner portions of the preparation become blue-gray. In the second DSC endotherm region (220–250 °C), the viscosity again decreases and the nematic phase appears with readily identifiable Schlieren and homeotropic textures. When cooled to the N/ S_{x2} transition, growth of bâtonnets and formation of small spherulites can be observed. As the temperature is further decreased, the spherulites progressively disappear. At ca. 185–175 °C (S_{x1}/S_{x2} transition), textural changes occur and the spherulitic texture is replaced by small platelet-like domains of uniform color.

The crystalline phase is clearly evidenced by X-ray diffraction. At room temperature, the X-ray diffracto-

(34) Benattar, J. J.; Moussa, F.; Lambert, M. *J. Chim. Phys., Phys. Chim. Biol.* **1983**, *80*, 99.

(35) Kumar, S.; Le Grange, J.; McMillan, W. L.; Mochel, J. *Phys. Rev. A* **1982**, *25*, 2258.

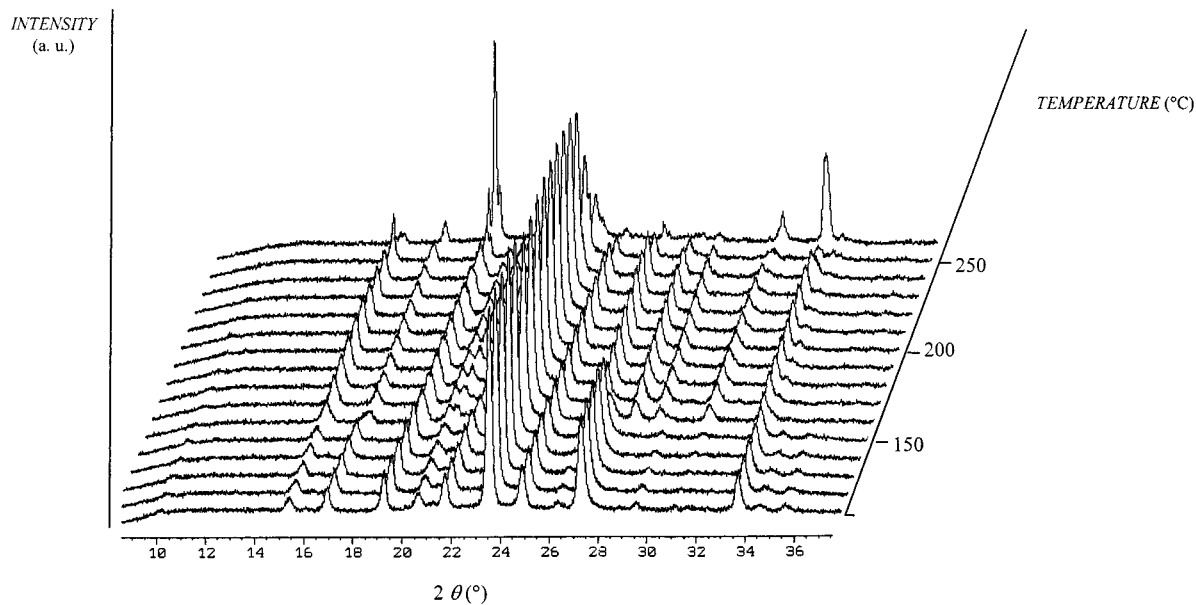


Figure 6. Time-dependent X-ray diffraction plots (TDXD) for compound **3** in air.

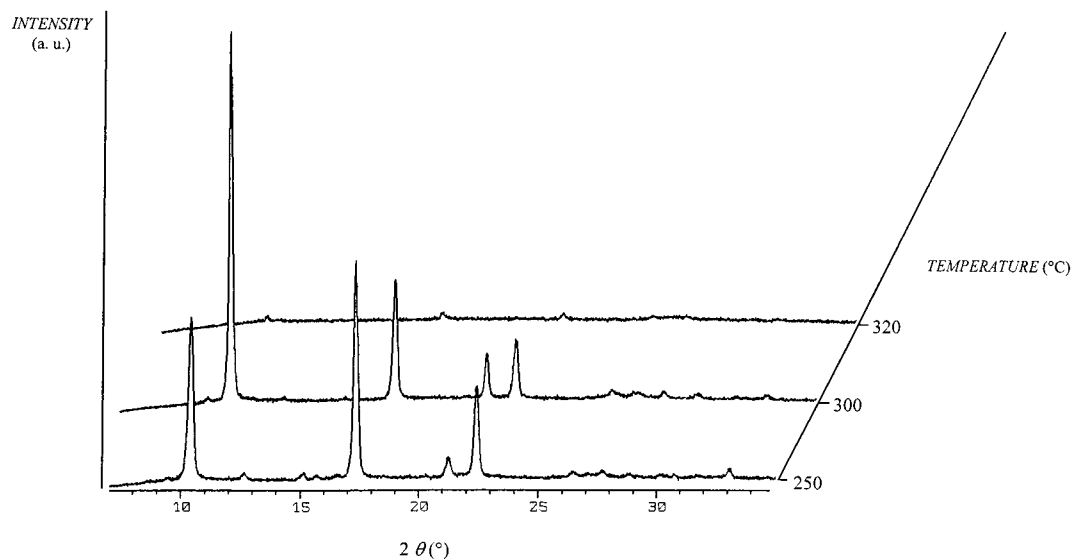


Figure 7. Time-dependent X-ray diffraction plots (TDXD) for compound **4** in air.

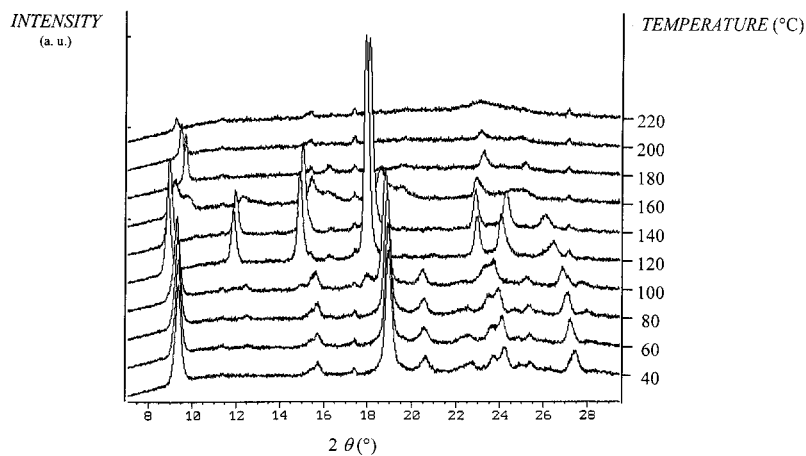


Figure 8. Time-dependent X-ray diffraction plots (TDXD) for compound **5** in air.

gram presents several well-defined peaks corresponding to the lattice spacing given in Table 5. From these data alone we are unable to confidently propose unit cell

parameters. It is worth noting, however, that the first four orders of reflection correspond to a repeat distance $d = 30.25 \text{ \AA}$, which is roughly equal to the extended

Table 4. *d* Spacings Measured from the TDXD Plots for Compound 5 in Air (*L* = 34.1 Å)

temp (°C)	<i>d</i> spacing(Å)
20	32.40 ^a 16.23 ^a 10.81 ^a 5.42 4.555 4.38 4.29 4.16 3.79 3.67
30	10.84 6.54 ^b 5.43 5.00 ^b 4.55 4.34 4.26 4.14 3.93 ^b 3.76 3.64
40	10.95 6.64 6.52 5.92 5.43 5.01 4.56 4.35 4.27 4.07 3.77
60	10.96 6.68 6.54 5.91 5.44 5.02 4.59 4.37 4.29 4.17 4.07 3.8
80	10.98 8.23 6.68 6.55 5.92 5.45 5.02 4.60 4.40 4.32 4.20 4.08 3.2
100	11.03 8.25 6.87 6.67 6.58 5.92 5.73 5.18 5.05 4.64 4.43 4.36 4.10 3.85
120	11.52 8.63 6.90 5.73 4.50 4.29 3.91 3.81
140	11.36 ^c 8.53 ^c 6.84 ^c 5.69 4.51 4.26 3.96
160	11.47 ^d 11.14 ^e 10.44 ^f 8.38 ^e 6.69 ^e 5.59 ^e 4.51 4.23 ^d 4.11 ^f
180	10.59 9.05 6.69 6.34 5.92 5.26 4.44 4.11 3.81
200	10.83 6.70 5.92 4.46 3.81
220	11.08 6.70 5.93 4.44 (diffuse halo) 3.81

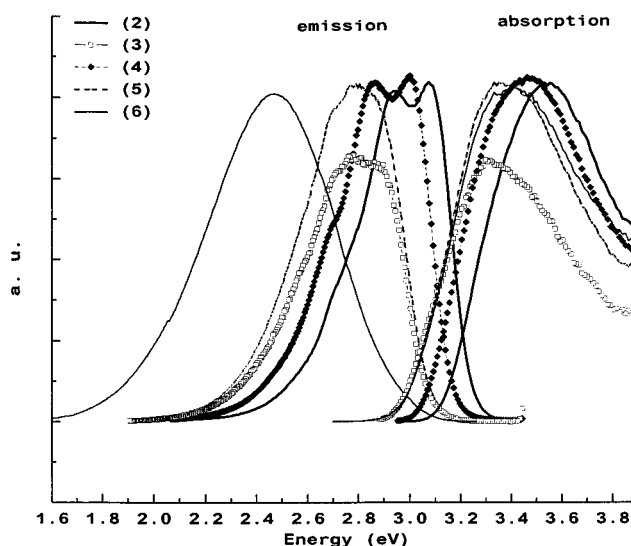
^a Base reflection, 001; second-order reflection, 002; and third-order reflection, 003, corresponding to a Bragg spacing of $d \approx 32.43$ Å. ^b Reflections of the K₂ phase. ^c Phase third-order reflection, 003; fourth-order reflection, 004; and fifth-order reflection, 005, corresponding to a Bragg spacing of $d \approx 34.13$ Å. ^d Reflections of the K₃. ^e Third-order reflection, 003; fourth-order reflection, 004; fifth-order reflection, 005; and sixth-order reflection, 006, corresponding to a Bragg spacing of $d \approx 33.48$ Å. ^f Reflections of the S_F phase.

Table 5. *d* Spacings Measured from the TDXD Plots for Compound 6 in Air (*L* = 30.54 Å)

temp (°C)	<i>d</i> spacing (Å)
20	30 ^a vs ^b 15.10 ^a s 10.13 ^a w 7.60 ^a m 5.94 w 4.97 s 4.30 m 3.755 s 3.63 m
120	4.29 s
140	4.30 s
160	4.32 s
180	4.33 s
200	4.35 s
220	4.37 ^c w
240	4.6 (diffuse halo)
260	4.6 (diffuse halo)

^a Base reflection, 001; second-order reflection, 002; third-order reflection, 003; and fourth-order reflection, 004, corresponding to a Bragg spacing of $d \approx 30.25$ Å. ^b vs, very strong; s, strong; m, medium; w, weak. ^c Very broad peak of low intensity.

molecular length $L = 30.54$ Å. The X-ray diffractograms do not change significantly with increasing temperature up to the melting point. A further increase in temperature results in a transformation of the X-ray diffractograms which are characterized in the wide-angle region by a strong peak at $d = 4.29$ Å (120 °C) to 4.35 Å (200 °C), suggesting a smectic B (S_B)-like structure. This reflection could be indexed as the 10 reflection of a 2D hexagonal lattice of parameter $a = 4.95$ –5.02 Å. The X-ray diffractograms show no evidence of *hkl* reflections. Hence, three-dimensional correlations are either absent or extremely weak in this smectic phase. The smectic period cannot be determined. Neither the base reflection nor higher order reflections on the layer planes can be detected in the X-ray diffractograms. It is worth noting that high polar substituents, e.g. CN or NO₂, induce new correlations (essentially of a dipolar nature) between molecules and favor an antiparallel arrangement of permanent dipoles. An overlapping head-to-tail arrangement of molecules would lead to a stacking period in excess of the extended molecular length L (but less than $2L$), i.e., too large to be

**Figure 9.** Optical absorption and photoluminescence spectra of compounds 2–6 in a mixture of toluene and acetonitrile (50/50 v/v).

determined under our experimental conditions ($2\theta > 7^\circ$, $d < 14.66$ Å). Over the temperature range 120–220 °C, the reflection shifts to progressively lower angles and gradually broadens and weakens in intensity. At 220 °C, in the S_{x2} phase, only a weak broad peak appears at $d = 4.37$ Å, indicating that the layers are less structured than in the S_{x1} phase or even liquidlike as in S_A phases. At above 240 °C, in the N phase, only a broad, diffuse halo is observed at $d \approx 4.6$ Å.

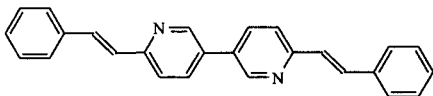
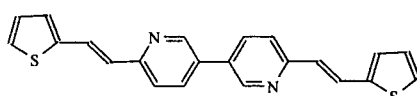
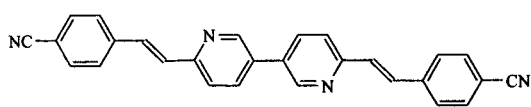
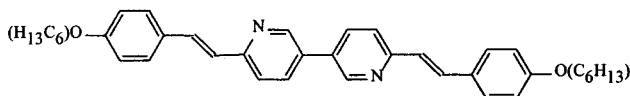
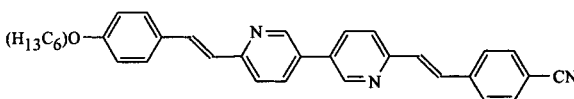
Linear Optical Properties. The linear optical data (i.e., absorption and emission maxima, molar extinction coefficient (ϵ), and quantum yields of fluorescence) obtained for compounds 2–6 in solution with a mixture of toluene and acetonitrile (50/50 v/v) are reported in Table 6.

UV–Visible Absorption. The high values of the molar extinction coefficients reported in Table 6 indicate that this strong absorption corresponds to a π – π^* transition.

Absorption spectra are shown in Figure 9. They exhibit a single structureless and broad absorption peak which could come from a distribution of ring-torsional ground states. Both the replacement of the phenyl rings by thienyl rings, on one hand, and the para-disubstitution of 2 by electron-donating and/or electron withdrawing groups, on the other hand, lead to a slight red shift of the absorption maximum: 3.49 eV (355 nm) for 2 as compared to 3.29, 3.39, 3.32 and 3.34 eV (377, 365, 373, and 371 nm) for 3–6, respectively. This bathochromic effect mirrors an increase of the conjugation path length in the latter molecules, the π -electron delocalization along the entire unsaturated molecule being more or less influenced by the donor or acceptor character of the substituents.

Photoluminescence. Figure 9 compares the photoluminescence (PL) spectra of the compounds 3–6 to that of 2 in the region 1.5–3.4 eV (365–830 nm). In the latter, a structured emission is observed with two distinct peaks at ca. 3.08 and 2.93 eV, with a shoulder at about 2.77 eV. Symmetrical para-disubstitution of 2 by electron-withdrawing CN groups, to give 4, results in a small red-shift (0.06 eV) of the peaks. The electron-donating OC₆H₁₃ group in 5 induces a greater red-shift

Table 6. Main Features of Absorption and Emission Spectra for Compounds 2–6 in a Mixture of Toluene and Acetonitrile (50/50 v/v)

compound	absorption		emission		
	E_{\max} (eV)	ϵ $10^4 \text{ l.mol}^{-1} \cdot \text{cm}^{-1}$	$E_{\max}^{[a]}$ (eV)	Φ_f (%)	
	2	3.49	6.8	3.08, 2.93, 2.77 ^b	62
	3	3.29	4.6	2.93, 2.78, 2.62	10
	4	3.39	8.0	3.02, 2.87, 2.74 ^b	72
	5	3.32	4.6	2.92, 2.77, 2.61	27
	6	3.34	2.8	2.45	50

^a Obtained by deconvolution of the emission spectrum. ^b Shoulder.

(0.16 eV). In this case, however, the PL spectrum broadens so that only two major peaks are discernible. Similar effects are observed when the phenyl rings are replaced by thienyl rings, again indicating that the latter act also as electron-donating groups.

As shown in Table 6, the main distance between component peaks of each spectrum is on average 0.16 eV for compounds 2–5. This value agrees with the energy of the intense absorption bands observed in the Raman spectra between 1600 and 1100 cm^{-1} (0.14–0.2 eV). These bands are most probably due to phenyl and heterocyclic C=C stretching and C–H bending, which suggests that the structured feature of the emission spectra arises from these vibronic couplings in the ground state.

The emission spectrum of **6** is quite different. The asymmetrically para-disubstituted compound is found to emit a broad and structureless band in the range 1.5–2.90 eV (430–830 nm), with a maximum at 2.45 eV. This long-wavelength fluorescence band could be attributed to an intramolecular charge-transfer (ICT) state emission involving the whole molecule. Such an assumption is supported by the large shift (ca. 3000 cm^{-1}) in the position of the fluorescence maximum observed by varying the solvent polarity when chloroform is replaced by acetonitrile.

More information about this phenomenon and the photophysical and electrochemical properties of the compounds will be reported in a future paper.³⁶

Conclusions

Starting from a 3,3'-bipyridine core leads easily, by Knoevenagel condensation with differently substituted

aromatic aldehydes, to highly π -conjugated molecules which can find applications in optoelectronics. This is specially the case with the donor–acceptor para-disubstituted compound **6**, which gives rise to a charge-transfer phenomenon, allowing it to be active in NLO. Hyperpolarizability β measurements are under investigation. In addition, formation of mesophases, a general characteristic of these molecules, is an advantage of this application. The use of benzaldehydes bearing reactive functional groups (for instance 4-hydroxybenzaldehyde) offers the opportunity to synthesize reactive chromophores able to be grafted on macromolecular chain, with a view to obtain SCLCPs exhibiting NLO properties. This approach is now also being investigated.³⁷

Besides, the photoluminescence, another property exhibited by most compounds, could be used for LED design, as will be described in a later paper.³⁸

Acknowledgment. The authors thank Dr. M. Jouini (Institut de Topologie et de Dynamique des Surfaces, Université de Paris 7) and Dr. P. Hapiot (Laboratoire d'Electrochimie Moléculaire, Université de Paris 7) for assistance in performing linear optical characterizations. Drs. G. Horowitz and P. Valat (Laboratoire des Matériaux Moléculaires–CNRS–Thiais) are also gratefully acknowledged for many helpful discussions throughout the preparation of the manuscript.

Supporting Information Available: Figure 1S (solid FT-Raman spectrum of **4** over the range from 3400 to 200 cm^{-1}), and Figure 2S (^{13}C NMR spectra of **4** in CDCl_3 , recorded by using the INEPT pulse sequence with (a) $J = 165 \text{ Hz}$ and (b) $J = 13 \text{ Hz}$). This material is available free of charge via the Internet at <http://pubs.acs.org>.

CM9811242

(36) Attias, A.-J.; Hapiot, P.; Valat, P.; Wintgens, V.; Horowitz, G. To be published.

(37) Lemaître, N.; Attias, A.-J.; Noël, C. To be published

(38) Attias, A. J.; Bacsá, W.; Zuppiroli, L. To be published.